Scientific paper

Green Synthesis of Co-alginate and CoNi-chitosan Catalysts for Catalytic Reduction of Organic Azo Dyes

Filiz Akti*

Department of Chemical Engineering, Hitit University, Corum 19030, Turkey

** Corresponding author: E-mail: filizakti@hitit.edu.tr*

Received: 02-16-2024

Abstract

Cobalt and nickel doped catalysts were synthesized by using chitosan and alginate and used in the degradation of Remazol Yellow 4GL (RY) and Remazol Black B (RB) dyes. XRD pattern of catalysts exhibited that amorphous and semi-crystalline form for CoNi-chitosan and Co-alginate, respectively. SEM images showed catalyst's surface was rough, grainy and rod-like structures. The surface functional groups were determined by FTIR analysis method and it was seen clearly presence of alginate and chitosan. The Co-alginate catalysts exhibited higher dye degradation (74% for RY) and lower reaction time (6 min for RB). The reduction reaction was in good agreement with pseudo-first-order kinetic model and reaction rate constant was determined as 0.140 min^{-1} and 0.174 min^{-1} for RY and RB, respectively. The RY reduction percent over both catalysts was higher than RB. Co-alginate showed approximately 70% reduction efficiency for RY even after 4 runs. The dye reduction efficiency and catalytic activity of the catalysts were promise for organic pollutant dyes catalytic reduction applications.

Keywords: Remazol Yellow 4GL; Remazol Black B; cobalt/nickel bead catalyst; catalytic reduction

1. Introduction

Dyes are widely used in textile, cosmetics, paper, leather, food, plastic and many other industries. Azo dyes (–N=N– group) are among the most harmful dyes due to their high physicochemical stability.[1] From these azo dyes, Remazol Yellow 4GL (RY) and Remazol Black B (RB) is a synthetic highly toxic dyes with a diazo group of symmetrical aromatic nature. They pose significant risks to human health such as mutagen, carcinogen, respiratory disorder, skin irritation and allergic reactions.[2–8] Their discharge to water pollutes both environment and threat to human and many vivid species health due to their toxic, carcinogenic and mutagenic properties.[9–13] Therefore, require efficient treatment before being released into aqueous media. Many methods such as adsorption, advanced oxidation, coagulation and reverse osmosis have been used for the treatment of wastewater containing organic dyes. Adsorption process is the most effective and reliable technique for removal of dyes from wastewater. Although adsorption has the advantage of high processing efficiency, ease of use, and relatively low cost, it is difficult to remove contaminants from the adsorbent. In recent years, the chemical reduction strategy using $NaBH_4$ in the presence of suitable catalysts has gained more and more research attention due to its advantages of environment friendly, low cost, high efficiency and easy operation. This process, while thermodynamically favorable, is kinetically unfavorable.[14–21] Therefore, electrons need a catalyst for their rapid transfer from borohydride ions to dye molecules.[22] Moreover, there may be a large redox potential difference between the electron donor (BH_4^- ion) and acceptor (dyes) species and this is also can hinder relaying of electrons. Metal nanoparticles (MNPs) are feasible enough to reduce the potential difference due to their high Fermi potentials for which they can exhibit excellent dye degradation efficiency. Au, Pt, Pd and Ag noble metal nanoparticles have been utilized in catalytic dye degradation due to their good electron transfer capabilities resulting from favorable redox potentials. However, they are expensive, which greatly limits their industrial applications. Co, Ni, Fe and Cu transition metals having low cost are good candidates to replace the noble metals.[16,23–26] The biggest obstacle to the use of these metal nanoparticles is instability and agglomeration problem that causes the reduction of their active sites due to their high surface energy. Also, they cannot be easily separated from the reaction medium, and this restricts their large-scale applications. To overcome this problem, many polymeric hydrogel networks, support materials such as SBA-

15, biochar, graphene have been used in preparation of metal nanoparticles.[9,15,27–33] Chitosan and alginate which are a natural biodegradable polysaccharide having non-toxic, environmentally friendly, is used for providing of polymeric hydrogel networks. Both of them provides excellent chelating ability and binding capacity to divalent metal cations thanks to its functional groups (RCOO–, OH–, CO–, NH_2–).[15,28,34,35] This attractive crosslinking character ensures them various shapes such as bead and membrane, as well as it make them more attractive for environmental applications which are adsorption, filtration, oxidation and catalytic reduction of organic pollutants.[15]

In the removal of RB and RY from wastewater adsorption and photocatalytic methods are generally used[2–8,36], while the use of catalytic reduction method is encountered. In study performed by Almeida et al. RB has been degraded photocatalytically using electric arc furnace dust and provided catalytic performance and degradation time of 81% and 150 min.[7] Secundino-Sánchez et al., have been declared that RB was degraded 50% and at 20 min in the presence of TiO_2-NF's-anatase photocatalysts.[4] In other work[5], GO/$CoFe_2O_4$ photocatalyst has been used for degradation of RB and observed 53% degradation efficiency within 60 min. On the other hand, there are very limited studies for the removal of RY. One of these studies is the study conducted by Akti[7] and the other is the study conducted by Akti and Balci.[8] Photocatalytic method was used in these studies. Akti removed 96% of RY in 60 min using PANI-SnO_2@diatomite, while Akti and Balci removed 58.2% in 150 min.[7,8] All these materials have exhibited promising results in removing pollutants from wastewater. However, there is still a need for effective, cheap, economical, environmentally friendly and non-toxic catalysts.

This paper deal with the synthesis, characterization and activity test of chitosan and alginate network-structured cobalt and cobalt-nickel bead type catalysts for catalytic reduction of RY and RB, selected as a model pollutant. The novelty of the present study lies in the fact that the synthesized catalysts have been reported in a limited number of studies in the literature for reduction, and their catalytic activity is highly competitive.

2. Materials and Methods

2. 1. Materials

$CoCl_2.6H_2O$ (≥ 95%), $NiCl_2.6H_2O$ (≥ 95%), sodium alginate, chitosan (low molecular weight), $CaCl_2$ (≥ 93%) and NaOH (≥ 99%) were supplied from Sigma-Aldrich. Acetic acid (glacial 100%) and $NaBH_4$ (≥ 98%) were taken Isolab and Merck, respectively. The Remazol Yellow 4GL (C. I. Reactive Yellow 160; $C_{25}H_{22}ClN_9Na_2O_{12}S_3$) and Remazol Black B (C. I. Reactive Black 5; $C_{26}H_{21}N_5Na_4O_{19}S_6$) were obtained from a local textile company in Turkey. All chemicals were of analytical grade and were used directly.

2. 2. Synthesis of Co-alginate and CoNi-chitosan Bead Type Catalysts

Co-alginate bead type catalysts synthesis; 0.2 g $CoCl_2.6H_2O$ was dissolved in 50 mL distilled water, 1 g of sodium alginate (2 w/v%) added and mixture was stirred for 3h at room temperature. Afterward obtained gel was dropped into 100 mL of 1% (w/v) $CaCl_2$ solution using a syringe for bead formation and stirred at 150 rpm for 2 h for stable structure. And then formed beads were filtered, rinsed several times with distilled water for remove unreacted $CaCl_2$ and dried at room condition.

CoNi-chitosan bead type catalysts synthesis; 0.1 g $CoCl_2.6H_2O$ and 0.1 g $NiCl_2.6H_2O$ were dissolved in 50 mL acetic acid (1 v/v%) and added a solution containing 2% chitosan (w/v). The mixture was stirred for 3 h at room temperature and then dropped into 100 mL of 1 M NaOH solution with a syringe. The occurred beads were kept in NaOH solution at 150 rpm for 2 h for stable structure and then filtered, washed several times with distilled water for remove unreacted NaOH on the surface of beads and dried at room condition.

2. 3. Characterization of Co-alginate and CoNi-chitosan Bead Type Catalysts

X-ray diffraction (XRD) patterns were taken in the 2θ range of 10–90° with 0.02° step size and scan speed of 1°/min using Philips PW 3040 device with CuKα radiation (λ = 0.15406 nm). The crystallite sizes (D) of metal species within polymer matrix were determined from Debye Scherrer equation ($D = 0.9\ \lambda)/(\beta\cos\theta)$) where β is full width half maximum (FWHM) of the strongest peak corresponding to metal species.[37]

Scanning electron microscopy (SEM) images were taken on Quanta 400F Field Emission model electron microscope at 30 kV. Before the analysis samples were attached on carbon tape and covered with a very thin layer of Au-Pd.

Fourier transforms infrared (FTIR) spectra (resolution of less than 0.09 cm^{-1}) were recorded on a Thermo Scientific/Nicolet IS50 instrument with a Pike ATR (attenuated total reflectance) adapter. FTIR data were collected with 0.5 cm^{-1} increment in the wavelength range of 600–4000 cm^{-1}.

2. 4. Catalytic Activity Evaluation of Co-alginate and CoNi-chitosan Bead Type Catalysts

The activity of the catalysts was tested in the reduction reaction of Remazol Yellow 4GL (RY) and Remazol Black B (RB) dyes in the presence of $NaBH_4$. All solutions were freshly prepared before reaction test. 1.5 mL of dye solution (20 mg/L) and 1 mL of $NaBH_4$ solution (0.3 M) were mixed. And then mixture was taken to a quartz cuvette, followed by addition of 30 mg of catalyst. Catalytic

reduction was monitored at regular intervals of time using a Thermo Scientific/Evolution-201 UV-vis spectrophotometer in the wavelength range of 200–700 nm. Kinetic data were collected by measuring the absorbance values of RY and RB dye solutions at 429 nm and 562 nm, respectively. The kinetics of the reduction were investigated by implying the reaction process pursuing the pseudo-first order and pseudo second-order law, with the following equations: Eqs. (1) and (2), respectively. Reduction rate % was calculated using Eq. (3).

$$\ln\left(\frac{A_t}{A_o}\right) = -k_{app}t \quad (1)$$

$$1/A_t = -k_{app}t \quad (2)$$

$$\text{Reduction rate } \% = (A_o - A_e)/A_o x100 \quad (3)$$

Where k_{app} (min^{-1}) is the rate constant, A_t is absorbance at time t, A_o is initial absorbance and A_e is absorbance at equilibrium of dye solutions.

3. Results and Discussion

3. 1. Characterization of Catalysts

XRD patterns are given in Fig. 1. Co-alginate exhibited semi-crystalline structure while CoNi-chitosan showed an amorphous structure. The semi-crystallinity due to chitosan derives from the presence of inter- and intramolecular hydrogen bonds between the hydroxyl and amine groups on glucosamine units that lead to the formation of parallel and closely packed polymer chains.[38] Two broad peaks corresponding to crystalline plane of chitosan were obtained at ~ 20° and 40° Bragg angle values for Co-Ni-chitosan[39,40]. No obvious diffraction peaks related to the cobalt and nickel phases were obtained due to the metals might be embedded/settled as very small particle to the chitosan structure. Co-alginate exhibited oxide (2θ: 29.14°, 33.96° and 36.98°) and metallic (2θ: 44.54°) forms of cobalt species[41,42] and crystallite size of cobalt was calculated as 25.12 nm from the highest peak intensity at 33.96 ° by Scherrer equation.

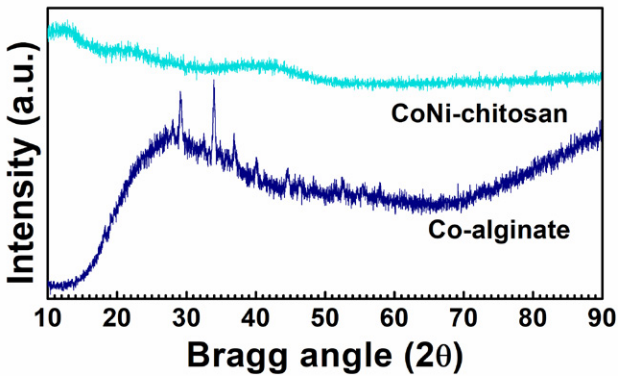

Figure 1. XRD patterns of Co-alginate and CoNi-chitosan bead type catalysts.

Fig. 2 shows the surface morphology of Co-alginate and CoNi-chitosan. Grainy structure of 4–25 µm size were observed on the surfaces of catalysts (Fig. 2a and c). It was observed that the surface of CoNi-chitosan (Fig. 2d) was rougher than Co-alginate (Fig. 2b). In addition to, grainy and rod-like structures were also observed for CoNi-chitosan. This different morphological structure may be related to the interaction between metals and alginate and chitosan.

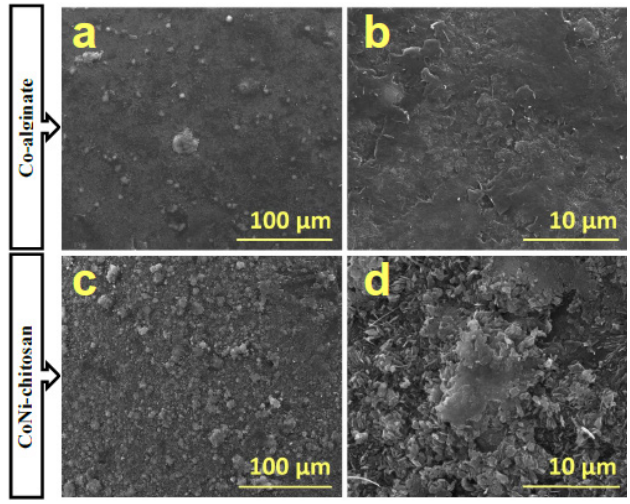

Figure 2. SEM images bead type catalysts of Co-alginate (**a, b**) and CoNi-chitosan (**c, d**).

FTIR spectrums of catalysts are shown in Fig. 3. The peak at 850 cm^{-1} related to the C–H band in the chitosan structure. The peak observed at around 1030 cm^{-1} indicates the C–O vibration, while the peaks obtained at 1350 cm^{-1} and 1460 cm^{-1} shows the C–H vibration originating from the CH_2/CH_3 groups. The peak detected at 1644 cm^{-1} was assigned the C=O bond found in chitosan and

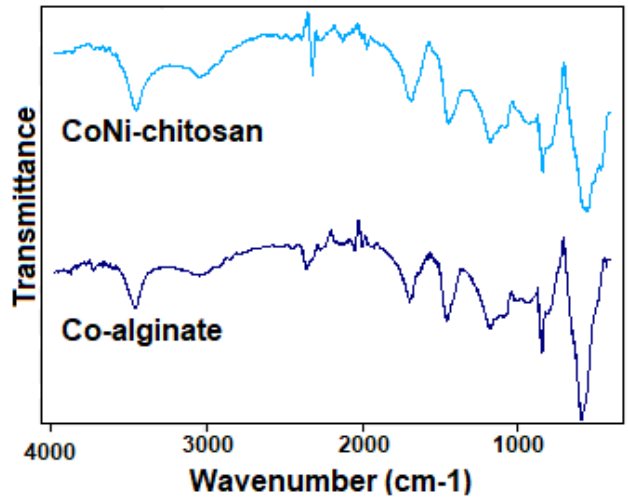

Figure 3. FTIR spectrums of Co-alginate and CoNi-chitosan bead type catalysts.

alginate structures. Addition, the N–H groups of chitosan were observed at 1557 cm^{-1} and 3270 cm^{-1} wavenumbers. The peak obtained at approximately 3450 cm^{-1} is due to the O–H band in the structure of chitosan and alginate.[40,43–46]

3. 2. Catalytic reduction of RY and RB over catalysts

The Co-alginate and CoNi-chitosan catalysts were tested in RY and RB reduction reaction and monitored results by UV-vis absorption spectra with time-dependent (Fig. 4). The dyes were reduced immediately in a short time. The rapid decrease in the absorption peaks observed at 429 nm and 562 nm clearly indicated the degradation of RY and RB, respectively. The reduction rate of RY in the first 2 min was about 18% for both catalysts. In total, RY was degraded by 74.0% in 10 min with Co-alginate and 50.4% in 6 min with CoNi-chitosan. RB degraded by 33% with CoNi–chitosan and by 4% with Co–alginate within the first 2 min. As can be predicted from the reduction in the absorption peak intensity at 562 nm, 66.4% and 21.9% of RB degraded by Co-alginate and CoNi-chitosan, respectively (Fig. 4a-d and Fig. 5b).

The difference in degradation performance of two dyes with different structures on different catalysts is due to the different physicochemical properties and molecular and electronic structures of the catalysts and dyes. It is well known that functional groups such as sulfonic (SO_3), hydroxyl (OH), methyl (CH_3), nitro (NO_2), and azo linkages (N=N) present in dye structures play a significant role in influencing the degradation process.[47–49] Khataee and Kasiri reported that monoazo dyes exhibited a higher degradation rate.[49] Rauf et al. stated that dye degradation occur primarily due to the cleavage of –N=N– azo bonds.[50] The –NH group in dye molecule is the fragile group. Besides, the sulfonic group may be increased the adsorb ability of the dye molecules on the catalyst contributing to higher degradation rate. On the other hand, the electron donating group attached

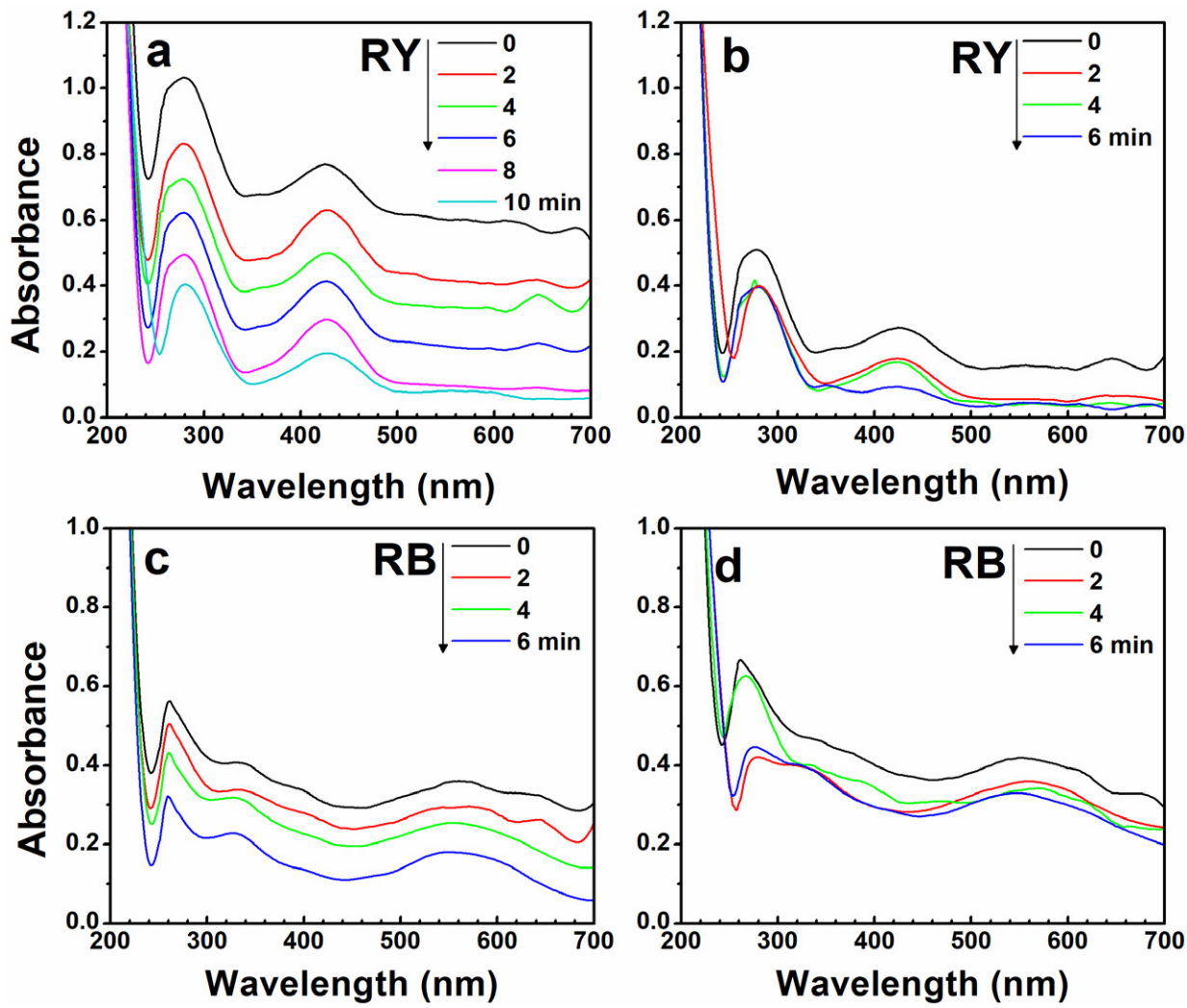

Figure 4. Time dependent UV–Vis absorption monitoring reduction of RY dye (**a:** Co-alginate, **b:** CoNi-chitosan) and RB dye (**c:** Co-alginate, **d:** CoNi-chitosan) over catalysts.

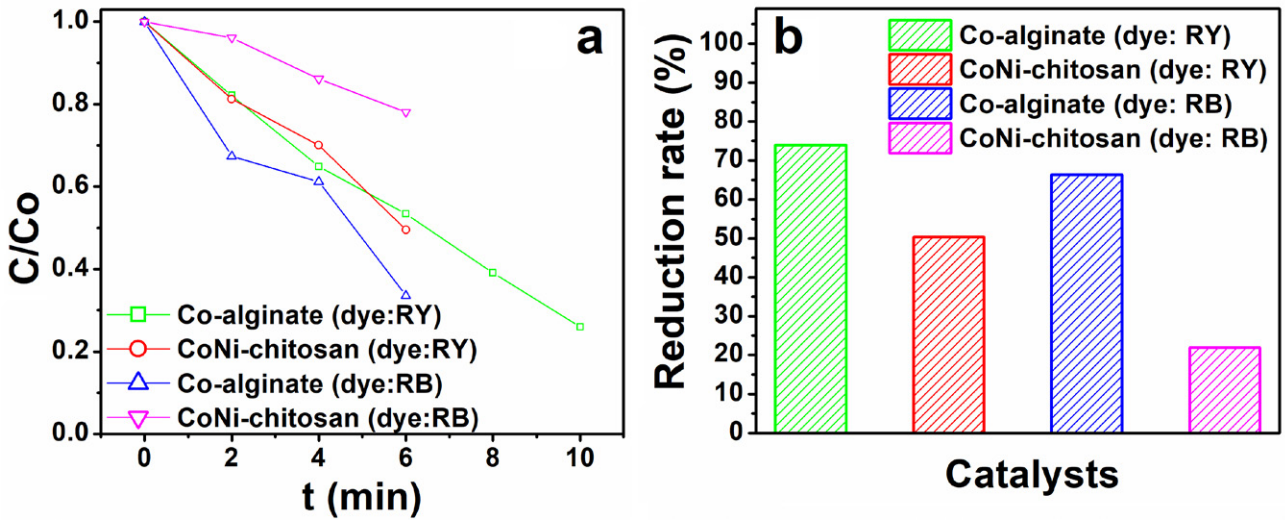

Figure 5. **(a)** The relationships of (C/C_o) versus reaction time **(b)** Reduction rate percent of dyes over catalysts.

to the molecular structure of dyes becomes more nucleophilic by donating some of its electron density.[48] Pervez et al. stated that the presence of $-CH_3$ group has a significant effect on the molecular mobility of dye molecules in the catalytic degradation of dyes.[47] Khataee and Kasiri explained that the number of –OH groups in dye molecule can increase the dye degradation rate.[49] Apart from these discussions, Von-Kiti et al. stated that the topological polar surface area (TPSA) of dyes is effective in dye removal, and that dyes with a low TPSA can show better removal performance.[51]

In the present study, the reduction rate of RY was found to be higher than that of RB. There could be several reasons for this. For example, RY is a monoazo dye (with a

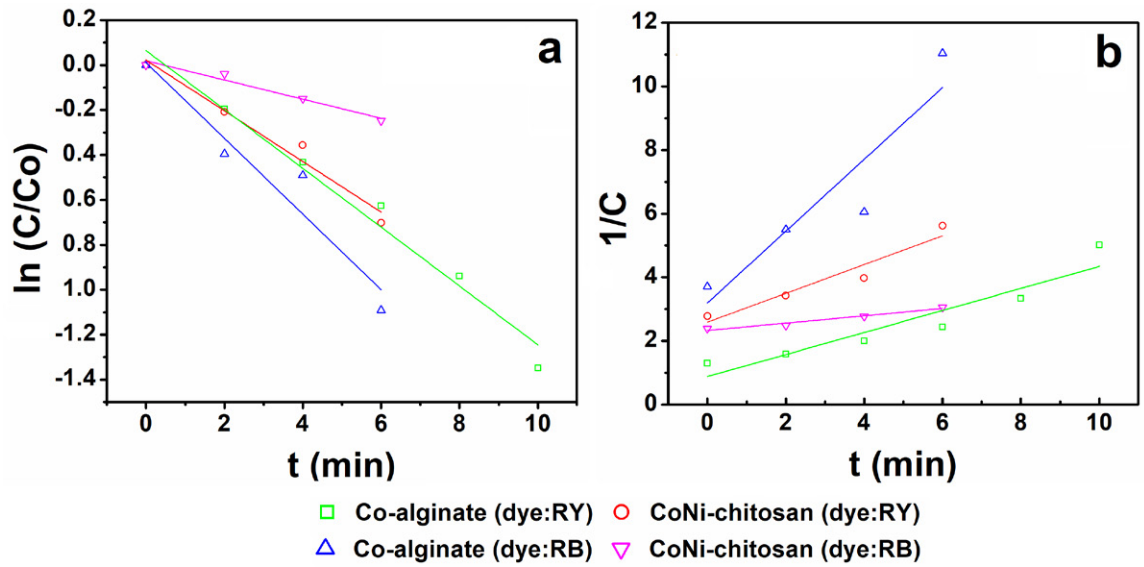

Figure 6. Kinetic plots of catalytic reduction of RY and RB dyes over Co-alginate and CoNi-chitosan bead type catalysts **(a)** first-order **(b)** second-order.

Table 1. Properties of dyes.

Dye	Properties							
	$N_{N=N}$	N_{SO3}	N_{OH}	N_{NH}	N_{CH3}	HBDC*	TPSA (Å)²*	Complexity*
Remazol Yellow 4GL	1	2	–	4	2	5	355	1720
Remazol Black B	2	4	1	1	–	2	462	2030

N: number of groups; *: Ref: https://pubchem.ncbi.nlm.nih.gov/

Table 2. First-order and second-order kinetic parameters for the reduction of RY and RB over catalysts.

Catalyst	Dye	Pseudo-first-order		Pseudo-second-order	
		k_{app} (min^{-1})	R^2	k_{app} ($Lg^{-1}min^{-1}$)	R^2
Co-alginate	Remazol Yellow 4GL	0.140	0.979	0.346	0.887
CoNi-chitosan	Remazol Yellow 4GL	0.124	0.969	0.452	0.928
Co-alginate	Remazol Black B	0.174	0.930	1.127	0.860
CoNi-chitosan	Remazol Black B	0.052	0.968	0.115	0.960

single –N=N– bond), and it has a higher number of –NH and $–CH_3$ groups compared to RB. Additionally, the hydrogen bond donor count (HBDC) of RY is higher than that of RB. Moreover, the topological polar surface area (TPSA) and complexity values of RY are lower than those of RB. Although RB has a higher number of SO_3 and –OH groups compared to RY, its lower removal percentage may be due to the reduced interaction between the catalyst and the dye molecules, or its higher complexity and greater number of N=N groups (Table 1).

To discuss the kinetics of the dye reduction, pseudo-first-order and pseudo-second-order kinetic models were applied.[52,53] The k_{app} values were estimated from the slope of the lines in Fig. 6. The rate constants and coefficients of determination (R^2) calculated for the models are presented in Table 2. As the kinetic models were compared, kinetic data fitted well pseudo-first-order kinetic model ($R^2 \leq 0.979$). The k_{app} values for RY were found to be 0.140 and 0.124 min^{-1} for the Co-alginate and Co-Ni-chitosan, respectively and for RB as 0.174 and 0.052 min^{-1}. Both higher dye reduction and a higher reaction rate constant were obtained with Co-alginate. Possible reasons for this include the combination of cobalt with alginate may be improve the steric structure inside the alginate, thereby increasing the adsorption of dye onto the catalyst surface.[35]

Reusability test was performed for Co-alginate in degradation of RY. Firstly, the catalyst was easily collected after completing of reaction thanks to their bead shape, washed with deionized water and then reused under the same reaction conditions. The catalyst could be successfully recycled up to 4 runs and the reduction efficiency of RY was determined as 70% even after 4 runs (Fig. 7).

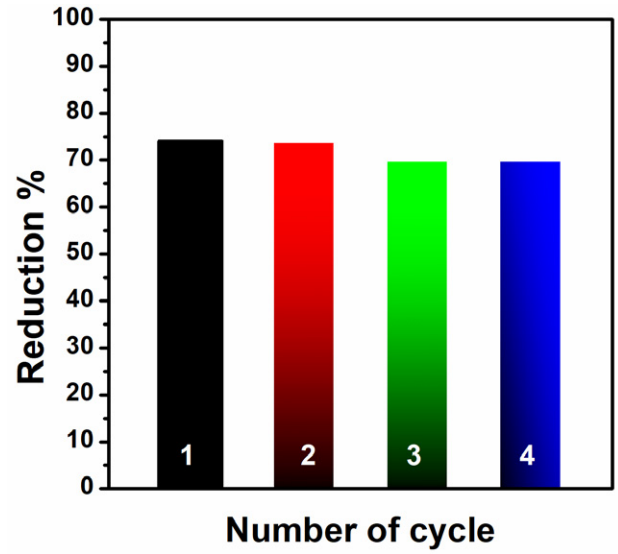

Figure 7. Reusability of Co-alginate for RY dye.

The dye reduction performance of the synthesized catalysts was compared with that of different materials and

Table 3. The catalytic degradation reaction kinetic of RY and RB over different catalysts.

Sample	Dye	Dye concentration (mg/L)	Degradation method	Degradation (%)	Degradation time (min)	k_{app} (min^{-1})	Reference
Co-alginate	Remazol Yellow 4GL	20	Catalytic reduction	74.0	10	0.140	This work
CoNi-chitosan	Remazol Yellow 4GL	20	Catalytic reduction	50.4	6	0.124	This work
PANI-SnO_2@Diatomite	Remazol Yellow 4GL	50	Photocatalytic	96.0	60	0.042	7
Sn/SBA-15@APTES(EA)	Remazol Yellow 4GL	50	Photocatalytic	58.2	150	0.0016	8
α-Fe_2O_3 NPs	Remazol Yellow RR	50	Photocatalytic	75.0	250	0.006	54
Fe^{2+} ions	Remazol Yellow FG	100	Contact glow discharge electrolysis	51.3	180	–	55
Co-alginate	Remazol Black B	20	Catalytic reduction	66.4	6	0.174	This work
CoNi-chitosan	Remazol Black B	20	Catalytic reduction	21.9	6	0.052	This work
Electric arc furnace dust	Remazol Black B	40	Photocatalytic	81.0	150	0.002	2
TiO_2-NF's-anatase	Remazol Black B	20	Photocatalytic	50.0	20	0.068	4
GO/$CoFe_2O_4$	Remazol Black B	10	Photocatalytic	53.0	60	0.102	5

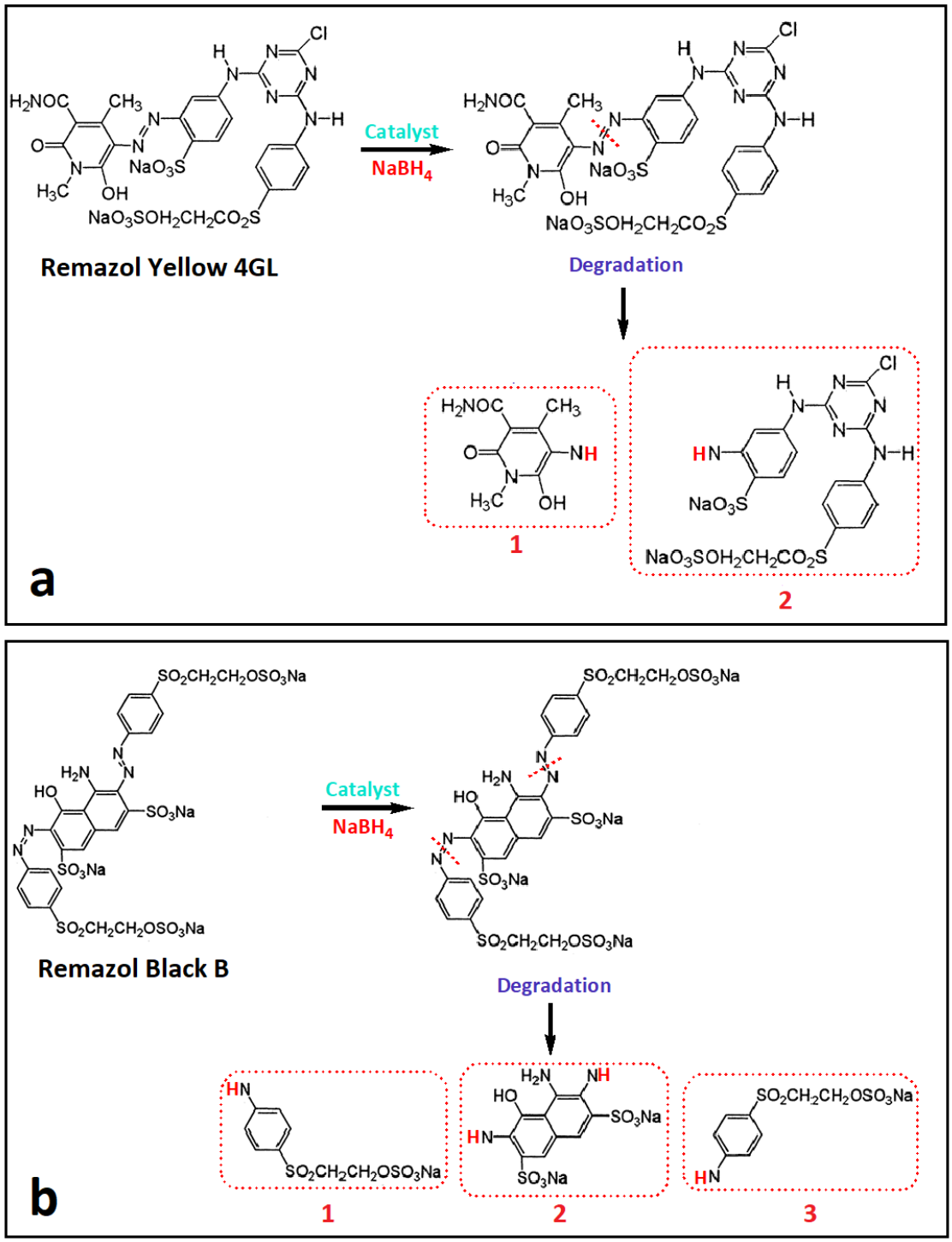

Scheme 1. Possible mechanism of reduction reaction of two dyes by catalysts.

reduction methods, and the results are presented in Table 3. In the present study, both high reduction capacity and a high reaction rate constant value were achieved with the synthesized catalysts, and it was observed that reduction or degradation occurred in a shorter time. From this perspective, it can be said that the catalysts are promising for dye reduction.

3. 3. Possible Catalytic Reduction Mechanism of RY and RB Dyes

The reduction reaction of dyes in the presence of $NaBH_4$ proceeds via Langmuir–Hinshelwood mechanism, where the reaction occurs due to interaction between adsorbed species (both dye and reductant). In this dye reduc-

tion process, the first step involves the diffusion of reactants into the pores of catalysts, and it is generated that electrons from $NaBH_4$ and hydrides from aqueous media. In the second step, these electrons and active hydride species are transferred to metal nanoparticles, resulting in the formation of metal–hydride bonds. Dye molecules incline to capture hydrogen and electrons from the metal–hydride complex.[26,56–59] According to the previously reported literature studies[19,26,59–62], the possible mechanism of dye reduction by catalyst and resulting products are proposed in Scheme 1. The H atom attaches to the N atom of heterocyclic ring in dye and breaks down azo double bond (–N=N–) between N and aromatic ring via conjugation. The broken bonds reduce to hydrazine group (–HN–NH–) and convert to products. The products occur according to azo double bond number of RY (single azo class) and RB (double azo class) (Scheme 1a and 1b).

4. Conclusion

Co-alginate and CoNi-chitosan catalysts were successfully designed for the catalytic reduction of RY and RB dyes. Co-alginate demonstrated high catalytic efficiency within a short time. The RY degraded 74% and 50% with Co-alginate and CoNi-chitosan, and also RB 66% and 22%, respectively. Different results were obtained with the same catalyst for RY and RB reduction. This behavior is thought to be due to the interaction between the dye and the catalyst. The rate constant, reaction time and reusability obtained in this study are quite assertive. The catalysts may serve as potential candidates not only for the dye reduction but also for the removal of various harmful organic and inorganic pollutants.

5. References

1. Alene, A. N.; Teshager, A. A.; Adugna, A. G.; Kndie, T. M.; Feleke, M. K.; Atlabachew, M.; Abate, G. Y.; Nguyen, D. T. A. Nanocatalytic reductive removal of Congo-red dye using boron-loaded cobalt oxide nanocomposites from aqueous solutions. *Results in Chemistry* **2025**, *15*, 102222. **DOI:**10.1016/j.rechem.2025.102222
2. Almeida, M. M.; Saczk, A. A.; da Silva Felix, F.; Penido, E. S.; Santos, T. A. R.; de Souza Teixeira, A.; Magalhães, F. Characterization of electric arc furnace dust and its application in photocatalytic reactions to degrade organic contaminants in synthetic and real samples. *Journal of Photochemistry and Photobiology A: Chemistry* **2023**, *438*, 114585. **DOI:**10.1016/j.jphotochem.2023.114585
3. Cardoso, N. F.; Pinto, R. B.; Lima, E. C.; Calvete, T.; Amavisca, C. V.; Royer, B.; Cunha, M. L.; Fernandes, T. H.; Pinto, I. S. Removal of remazol black B textile dye from aqueous solution by adsorption. *Desalination* **2011**, *269* (1–3), 92–103. **DOI:**10.1016/j.desal.2010.10.047
4. Secundino-Sánchez, O.; Díaz-Reyes, J.; Sánchez-Ramírez, J.; Arias-Cerón, J.; Galván-Arellano, M.; Vázquez-Cuchillo, O. Controlled synthesis of electrospun TiO2 nanofibers and their photocatalytic application in the decolouration of Remazol Black B azo dye. *Catalysis Today* **2022**, *392*, 13–22. **DOI:**10.1016/j.cattod.2021.10.003
5. Sheshmani, S.; Falahat, B.; Nikmaram, F. R. Preparation of magnetic graphene oxide-ferrite nanocomposites for oxidative decomposition of Remazol Black B. *International journal of biological macromolecules* **2017**, *97*, 671–678. **DOI:**10.1016/j.ijbiomac.2017.01.041
6. Shakeri, N.; Amooey, A. A.; Amoei, A.; Tahmasebizadeh, M. Evaluation of an Anaerobic/Aerobic System for Reactive Black 5 Removal: Kinetic Study. *Iranian Journal of Chemistry and Chemical Engineering* **2021**, *40* (5), 1512–1521.
7. Akti, F. Photocatalytic degradation of remazol yellow using polyaniline–doped tin oxide hybrid photocatalysts with diatomite support. *Applied Surface Science* **2018**, *455*, 931–939. **DOI:**10.1016/j.apsusc.2018.06.019
8. Akti, F.; Balci, S. Synthesis of APTES and alcohol modified Sn/SBA-15 in presence of competitive ion: Test in degradation of Remazol Yellow. *Materials Research Bulletin* **2022**, *145*, 111496. **DOI:**10.1016/j.materresbull.2021.111496
9. ALSamman, M. T.; Sanchez, J. Recent advances on hydrogels based on chitosan and alginate for the adsorption of dyes and metal ions from water. *Arabian Journal of Chemistry* **2021**, *14* (12), 103455. **DOI:**10.1016/j.arabjc.2021.103455
10. Suvarna, A. R.; Shetty, A.; Anchan, S.; Kabeer, N.; Nayak, S. Cyclea peltata leaf mediated green synthesized bimetallic nanoparticles exhibits methyl green dye degradation capability. *Bionanoscience* **2020**, *10*, 606–617. **DOI:**10.1007/s12668-020-00739-9
11. Balci, B.; Aksoy, N.; Erkurt, F. E.; Budak, F.; Basibuyuk, M.; Zaimoglu, Z.; Turan, E. S.; Yilmaz, S. Removal of a reactive dye from simulated textile wastewater by environmentally friendly oxidant calcium peroxide. *International Journal of Chemical Reactor Engineering* **2021**, *19* (11), 1231–1243. **DOI:**10.1515/ijcre-2021-0062
12. Benredjem, Z.; Barbari, K.; Chaabna, I.; Saaidia, S.; Djemel, A.; Delimi, R.; Douas, S.; Bakhouche, K. Comparative investigation on the removal of methyl orange from aqueous solution using three different advanced oxidation processes. *International Journal of Chemical Reactor Engineering* **2021**, *19* (6), 597–604. **DOI:**10.1515/ijcre-2020-0243
13. Ali, A.; Garg, U.; Khan, K. U.; Azim, Y. Removal of organic and inorganic pollutants using CSFe3O4@ CeO2 nanocatalyst via adsorption–reduction catalysis: A focused analysis on methylene blue. *Journal of Polymers and the Environment* **2022**, *30* (10), 4435–4451. **DOI:**10.1007/s10924-022-02522-1
14. Dorraj, M.; Sadjadi, S.; Heravi, M. M. Pd on poly (1-vinylimidazole) decorated magnetic S-doped grafitic carbon nitride: An efficient catalyst for catalytic reduction of organic dyes. *Scientific Reports* **2020**, *10* (1), 13440. **DOI:**10.1038/s41598-020-70457-5
15. Abdelkrim, S.; Mokhtar, A.; Djelad, A.; Hachemaoui, M.; Boukoussa, B.; Sassi, M. Insights into catalytic reduction of

dyes catalyzed by nanocomposite beads Alginate@ Fe3O4: Experimental and DFT study on the mechanism of reduction. *Colloids and Surfaces A: Physicochemical and Engineering Aspects* **2022**, *650*, 129595. **DOI:**10.1016/j.colsurfa.2022.129595

16. Zahid, M.; Segar, A. S. M.; Al-Majmaie, S.; Shather, A.; Khan, M. F.; Alguno, A. C.; Capangpangan, R. Y.; Ismail, A. Elettaria cardamomum seed extract synthesized silver nanoparticles for efficient catalytic reduction of toxic dyes. *Environmental Nanotechnology, Monitoring & Management* **2023**, *20*, 100809. **DOI:**10.1016/j.enmm.2023.100809
17. Khakyzadeh, V. Evaluation of the performance of a hybrid advanced oxidation process for degradation of organic pollutants in aqueous media. *International Journal of Environmental Analytical Chemistry* **2022**, 1–10.
18. Hachemaoui, M.; Mokhtar, A.; Abdelkrim, S.; Ouargli-Saker, R.; Zaoui, F.; Hamacha, R.; Habib Zahmani, H.; Hacini, S.; Bengueddach, A.; Boukoussa, B. Improved catalytic activity of composite beads calcium alginate@ MIL-101@ Fe3O4 towards reduction toxic organic dyes. *Journal of Polymers and the Environment* **2021**, *29* (12), 3813–3826. **DOI:**10.1007/s10924-021-02177-4
19. Wang, G.; Zhao, K.; Gao, C.; Wang, J.; Mei, Y.; Zheng, X.; Zhu, P. Green synthesis of copper nanoparticles using green coffee bean and their applications for efficient reduction of organic dyes. *Journal of Environmental Chemical Engineering* **2021**, *9* (4), 105331. **DOI:**10.1016/j.jece.2021.105331
20. Deng, L.; Ren, H.; Fu, L.; Liao, M.; Zhou, X.; Chen, S.; Wang, H.; Wang, L. Ferrous and manganese oxalate for efficient heterogenous-Fenton degradation of organic pollutants: composite active site and mechanism perception. *International Journal of Chemical Reactor Engineering* **2023**, (0). **DOI:**10.1515/ijcre-2023-0024
21. Heidari, H.; Aliramezani, F. Ni/Fe3O4@ nanocellulose and Ni/nanocellulose green nanocomposites: Inorganic-organic hybrid catalysts for the reduction of organic pollutants. *Iran. J. Chem. Chem. Eng. Research Article Vol* **2022**, *41* (10).
22. Naseem, K.; Farooqi, Z. H.; Begum, R.; Irfan, A. Removal of Congo red dye from aqueous medium by its catalytic reduction using sodium borohydride in the presence of various inorganic nano-catalysts: a review. *Journal of cleaner production* **2018**, *187*, 296–307. **DOI:**10.1016/j.jclepro.2018.03.209
23. Linxu, X.; Zhigang, Y.; Xue, S.; Jin, W.; Sisi, X.; Rupeng, L.; Feiyong, C. Facile synthesis of CuO/Co3O4 nanoribbons with excellent catalytic performance for reduction of organic dyes. *Solid State Sciences* **2022**, *134*, 107048. **DOI:**10.1016/j.solidstatesciences.2022.107048
24. Rahmani, A.; Rahmani, H.; Zonouzi, A. Sponge like M-doped Ni/NiO (M= Cu, Co) composites and their catalytic activity toward dye reduction. *Materials Today Communications* **2020**, *25*, 101304. **DOI:**10.1016/j.mtcomm.2020.101304
25. Ajmal, M.; Siddiq, M.; Al-Lohedan, H.; Sahiner, N. Highly versatile p (MAc)–M (M: Cu, Co, Ni) microgel composite catalyst for individual and simultaneous catalytic reduction of nitro compounds and dyes. *RSC Advances* **2014**, *4* (103), 59562–59570. **DOI:**10.1039/C4RA11667D
26. Moussadik, A.; Brigiano, F. S.; Tielens, F.; Halim, M.; Kacimi, M.; El Hamidi, A. Self-supported Ag nanoparticles on AgTi2 (PO4) 3 for hazardous dyes reduction in industrial wastewater. *Journal of Environmental Chemical Engineering* **2022**, *10* (1), 106939. **DOI:**10.1016/j.jece.2021.106939
27. Bao, Y.; Shao, L.; Xing, G.; Qi, C. Cobalt, nickel and iron embedded chitosan microparticles as efficient and reusable catalysts for Heck cross-coupling reactions. *International journal of biological macromolecules* **2019**, *130*, 203–212. **DOI:**10.1016/j.ijbiomac.2019.02.143
28. Kurczewska, J. Chitosan-montmorillonite hydrogel beads for effective dye adsorption. *Journal of Water Process Engineering* **2022**, *48*, 102928. **DOI:**10.1016/j.jwpe.2022.102928
29. Maslamani, N.; Khan, S. B.; Danish, E. Y.; Bakhsh, E. M.; Zakeeruddin, S. M.; Asiri, A. M. Carboxymethyl cellulose nanocomposite beads as super-efficient catalyst for the reduction of organic and inorganic pollutants. *International journal of biological macromolecules* **2021**, *167*, 101–116. **DOI:**10.1016/j.ijbiomac.2020.11.074
30. Vandarkuzhali, S. A. A.; Pachamuthu, M.; Srinivasan, V.; Mohamed, S. K.; Abd-Rabboh, H. S.; Hamdy, M. S.; Balamurugan, V. Efficient reduction of dyes to leuco form over silver nanoparticles on functionalised SBA-15 and aminoclay. *International Journal of Environmental Analytical Chemistry* **2020**, 1–14. **DOI:**10.1080/03067319.2020.1811257
31. Ajmal, M.; Demirci, S.; Siddiq, M.; Aktas, N.; Sahiner, N. Simultaneous catalytic degradation/reduction of multiple organic compounds by modifiable p (methacrylic acid-co-acrylonitrile)–M (M: Cu, Co) microgel catalyst composites. *New Journal of Chemistry* **2016**, *40* (2), 1485–1496. **DOI:**10.1039/C5NJ02298C
32. Daneshafruz, H.; Barani, H.; Sheibani, H. Palladium nanoparticles-decorated β-cyclodextrin–cyanoguanidine modified graphene oxide: a heterogeneous nanocatalyst for suzuki–miyaura coupling and reduction of 4-nitrophenol reactions in aqueous media. *Journal of Inorganic and Organometallic Polymers and Materials* **2022**, *32* (3), 791–802. **DOI:**10.1007/s10904-021-02218-4
33. Zarei, M.; Mohammadzadeh, I.; Saidi, K.; Sheibani, H. Fabrication of biochar@ Cu-Ni nanocatalyst for reduction of aryl aldehyde and nitroarene compounds. *Biomass Conversion and Biorefinery* **2024**, *14* (2), 2761–2776. **DOI:**10.1007/s13399-022-02490-5
34. Srivastava, V.; Choubey, A. K. Investigation of adsorption of organic dyes present in wastewater using chitosan beads immobilized with biofabricated CuO nanoparticles. *Journal of Molecular Structure* **2021**, *1242*, 130749. **DOI:**10.1016/j.molstruc.2021.130749
35. Sun, Y.; Li, Y.; Chen, B.; Wang, M.; Zhang, Y.; Chen, K.; Du, Q.; Wang, Y.; Pi, X. Methylene Blue Removed from Aqueous Solution by Encapsulation of Bentonite Aerogel Beads with Cobalt Alginate. *ACS omega* **2022**, *7* (45), 41246–41255. **DOI:**10.1021/acsomega.2c04904
36. Ahmadi, S.; Rahdar, A.; Rahdar, S.; Igwegbe, C. A. Removal of Remazol Black B from aqueous solution using P-γ-Fe2O3 nanoparticles: synthesis, physical characterization, isotherm,

kinetic and thermodynamic studies. *Desalination and water treatment* **2019**, *152*, 401–410. **DOI:**10.5004/dwt.2019.23978
37. Niemantsverdriet, J. W. *Spectroscopy in catalysis: an introduction*; John Wiley & Sons, 2007. **DOI:**10.1002/9783527611348
38. Vakili, M.; Deng, S.; Liu, D.; Li, T.; Yu, G. Preparation of aminated cross-linked chitosan beads for efficient adsorption of hexavalent chromium. *International journal of biological macromolecules* **2019**, *139*, 352–360. **DOI:**10.1016/j.ijbiomac.2019.07.207
39. Sowmya, A.; Meenakshi, S. Zr (IV) loaded cross-linked chitosan beads with enhanced surface area for the removal of nitrate and phosphate. *International Journal of Biological Macromolecules* **2014**, *69*, 336–343. **DOI:**10.1016/j.ijbiomac.2014.05.043
40. Abdeen Z, M. S., Mahmoud M Adsorption of Mn (II) ion on polyvinyl alcohol/chitosan dry blending from aqueous solution. *Environmental Nanotechnology, Monitoring & Management* **2015**, *3*, 1–9. **DOI:**10.1016/j.enmm.2014.10.001
41. Akti, F. Green synthesis of pistachio shell-derived biochar supported cobalt catalysts and their catalytic performance in sodium borohydride hydrolysis. *International Journal of Hydrogen Energy* **2022**, *47* (83), 35195–35202. **DOI:**10.1016/j.ijhydene.2022.08.101
42. Zhang, M.; Jia, L.; Zhang, Y.-h.; Li, W.; Li, J.-l.; Hong, J.-p. Preparation of highly dispersed silicon spheres supported cobalt-based catalysts and their catalytic performance for Fischer-Tropsch synthesis. *Journal of Fuel Chemistry and Technology* **2023**, *51* (5), 608–615. **DOI:**10.1016/S1872-5813(22)60078-1
43. Kumirska, J.; Czerwicka, M.; Kaczyński, Z.; Bychowska, A.; Brzozowski, K.; Thöming, J.; Stepnowski, P. Application of spectroscopic methods for structural analysis of chitin and chitosan. *Marine drugs* **2010**, *8* (5), 1567–1636. **DOI:**10.3390/md8051567
44. Lustriane, C.; Dwivany, F. M.; Suendo, V.; Reza, M. Effect of chitosan and chitosan-nanoparticles on post harvest quality of banana fruits. *Journal of Plant Biotechnology* **2018**, *45* (1), 36–44. **DOI:**10.5010/JPB.2018.45.1.036
45. Su, C.; Berekute, A. K.; Yu, K.-P. Chitosan@ TiO2 composites for the adsorption of copper (II) and antibacterial applications. *Sustainable Environment Research* **2022**, *32* (1), 1–15. **DOI:**10.1186/s42834-022-00138-7
46. Benali, F.; Boukoussa, B.; Benkhedouda, N.-E.-H.; Cheddad, A.; Issam, I.; Iqbal, J.; Hachemaoui, M.; Abboud, M.; Mokhtar, A. Catalytic Reduction of Dyes and Antibacterial Activity of AgNPs@ Zn@ Alginate Composite Aerogel Beads. *Polymers* **2022**, *14* (22), 4829. **DOI:**10.3390/polym14224829
47. Pervez, M. N.; Mishu, M. M. R.; Tanvir, N. P.; Talukder, M. E.; Cai, Y.; Telegin, F. Y.; Zhao, Y.; Naddeo, V. Insights into the structures and properties of dyes in the Fenton catalytic process for treating wastewater effluent. *Water Environment Research* **2023**, *95* (12), e10948. **DOI:**10.1002/wer.10948
48. Khalik, W. F.; Ho, L.-N.; Ong, S.-A.; Wong, Y.-S.; Yusoff, N. A.; Lee, S.-L. Revealing the influences of functional groups in azo dyes on the degradation efficiency and power output in solar photocatalytic fuel cell. *Journal of Environmental Health Science and Engineering* **2020**, *18*, 769–777. **DOI:**10.1007/s40201-020-00502-y
49. Khataee, A.; Kasiri, M. B. Photocatalytic degradation of organic dyes in the presence of nanostructured titanium dioxide: Influence of the chemical structure of dyes. *Journal of Molecular Catalysis A: Chemical* **2010**, *328* (1–2), 8–26. **DOI:**10.1016/j.molcata.2010.05.023
50. Rauf, M.; Meetani, M.; Hisaindee, S. An overview on the photocatalytic degradation of azo dyes in the presence of TiO2 doped with selective transition metals. *Desalination* **2011**, *276* (1–3), 13–27. **DOI:**10.1016/j.desal.2011.03.071
51. Von-Kiti, E.; Oduro, W. O.; Animpong, M. A.; Ampomah-Benefo, K.; Boafo-Mensah, G.; Kwakye-Awuah, B.; Williams, C. D. Evidence of electronic influence in the adsorption of cationic and zwitterionic dyes on zeolites. *Heliyon* **2023**, *9* (9). **DOI:**10.1016/j.heliyon.2023.e20049
52. Li, H.; Jiang, D.; Huang, Z.; He, K.; Zeng, G.; Chen, A.; Yuan, L.; Peng, M.; Huang, T.; Chen, G. Preparation of silver-nanoparticle-loaded magnetic biochar/poly (dopamine) composite as catalyst for reduction of organic dyes. *Journal of colloid and interface science* **2019**, *555*, 460–469. **DOI:**10.1016/j.jcis.2019.08.013
53. Veisi, H.; Joshani, Z.; Karmakar, B.; Tamoradi, T.; Heravi, M. M.; Gholami, J. Ultrasound assisted synthesis of Pd NPs decorated chitosan-starch functionalized Fe3O4 nanocomposite catalyst towards Suzuki-Miyaura coupling and reduction of 4-nitrophenol. *International Journal of Biological Macromolecules* **2021**, *172*, 104–113. **DOI:**10.1016/j.ijbiomac.2021.01.040
54. Bhuiyan, M. S. H.; Miah, M. Y.; Paul, S. C.; Aka, T. D.; Saha, O.; Rahaman, M. M.; Sharif, M. J. I.; Habiba, O.; Ashaduzzaman, M. Green synthesis of iron oxide nanoparticle using Carica papaya leaf extract: application for photocatalytic degradation of remazol yellow RR dye and antibacterial activity. *Heliyon* **2020**, *6* (8), e04603. **DOI:**10.1016/j.heliyon.2020.e04603
55. Budikania, T. S.; Afriani, K.; Widiana, I.; Saksono, N. Decolorization of azo dyes using contact glow discharge electrolysis. *Journal of Environmental Chemical Engineering* **2019**, *7* (6), 103466. **DOI:**10.1016/j.jece.2019.103466
56. Abay, A. K.; Chen, X.; Kuo, D.-H. Highly efficient noble metal free copper nickel oxysulfide nanoparticles for catalytic reduction of 4-nitrophenol, methyl blue, and rhodamine-B organic pollutants. *New Journal of Chemistry* **2017**, *41* (13), 5628–5638. **DOI:**10.1039/C7NJ00676D
57. Farooqi, Z. H.; Sultana, H.; Begum, R.; Usman, M.; Ajmal, M.; Nisar, J.; Irfan, A.; Azam, M. Catalytic degradation of malachite green using a crosslinked colloidal polymeric system loaded with silver nanoparticles. *International Journal of Environmental Analytical Chemistry* **2022**, *102* (16), 4104–4120. **DOI:**10.1080/03067319.2020.1779247
58. Khan, N.; Shahida, B.; Khan, S. A.; Ahmad, Z.; Saeeduddin; Sheikh, Z.; Bakhsh, E. M.; Alraddadi, H. M.; Fagieh, T. M.; Khan, S. B. Anchoring Zero-Valent Cu and Ni Nanoparticles on Carboxymethyl Cellulose-Polystyrene–Block Polyisoprene–Block Polystyrene Composite Films for Nitrophenol

Reduction and Dyes Degradation. *Journal of Polymers and the Environment* **2023**, *31* (2), 608–620. **DOI:**10.1007/s10924-022-02579-y

59. Mahmoud, M. E.; Amira, M. F.; Abouelanwar, M. E.; Salam, M. A. Green synthesis and surface decoration of silver nanoparticles onto δ-FeOOH-Polymeric nanocomposite as efficient nanocatalyst for dyes degradation. *Journal of Environmental Chemical Engineering* **2021**, *9* (1), 104697. **DOI:**10.1016/j.jece.2020.104697
60. Ali, A.; Garg, U.; Khan, K. U.; Azim Y. Removal and inorganic pollutants using $CSFe_3O_4$@ CeO_2 nanocatalyst via adsorption–reduction catalysis: A focused analysis on methylene blue. *Journal of Polymers and the Environment* **2022**, *30* (10), 4435–4451. **DOI:**10.1007/s10924-022-02522-1
61. Deka, J. R.; Saikia, D.; Cheng, T.-H.; Kao, H.-M.; Yang, Y.-C. Bimetallic AgCu nanoparticles decorated on zeolitic imidazolate framework derived carbon: An extraordinarily active and recyclable nanocomposite catalyst for reduction of nitroarenes and degradation of organic dyes. *Journal of Environmental Chemical Engineering* **2023**, *11* (3), 109777. **DOI:**10.1016/j.jece.2023.109777
62. Mallakpour, S.; Azadi, E.; Dinari, M. Mesoporous Ca-alginate/melamine-rich covalent organic polymer/cupric oxide-based microgel beads as heterogeneous catalyst for efficient catalytic reduction of hazardous water pollutants. *Journal of Environmental Chemical Engineering* **2023**, *11* (2), 109294. **DOI:**10.1016/j.jece.2023.109294

Povzetek

Katalizatorji, dopirani s kobaltom in nikljem, so bili sintetizirani z uporabo hitozana in alginata ter uporabljeni pri degradaciji barvil Remazol Yellow 4GL (RY) in Remazol Black B (RB). XRD vzorec katalizatorjev je pokazal amorfno obliko za CoNi-hitozan in polikristalinično obliko za Co-alginat. SEM slike so pokazale, da je bila površina katalizatorja groba, zrnata in z valjastimi strukturami. Površinske funkcionalne skupine so bile določene z metodo FTIR analize in jasno je bila opažena prisotnost alginata in hitozana. Katalizatorji Co-alginat so pokazali višjo degradacijo barvila (74% za RY) in tudi krajši čas reakcije (6 min za RB). Reakcija redukcije je bila dobro skladna s kinetičnim modelom pseudo-prvega reda, konstanta hitrosti reakcije pa je bila določena kot 0,140 min^{-1} za RY in 0,174 min^{-1} za RB. Delež redukcije RY z obema katalizatorjema je bila višja kot pri RB. Co-alginat je pokazal približno 70% učinkovitost redukcije za RY celo po 4 ponovitvah. Učinkovitost redukcije barvila in katalitska aktivnost katalizatorjev obetata možnosti za aplikacije katalitske redukcije organskih onesnaževalnih barvil.